Brief Report

Dispersive Propagation of Terahertz Pulses in a Plasmonic Fiber

Nikolai I. Petrov

Scientific and Technological Centre of Unique Instrumentation, Russian Academy of Sciences,
117342 Moscow, Russia; petrovni@mail.ru

Abstract: The dispersion properties of surface plasmon polaritons (SPPs) during propagation on metal wires with a dielectric coating in the terahertz frequency range were investigated theoretically. An analytical expression was obtained for a pulsed electric field using the solution of Maxwell equations taking into account high-order dispersion terms. The influence of the dielectric coating on the distortion of the pulse shape was investigated. Unlike uncoated wire, the propagation of surface plasmon pulses along a coated wire is highly dispersive. It was shown that the coating leads to the appearance of a long-chirped signal with a propagation of only a few millimeters, i.e., when a terahertz pulse propagates along a coated wire, it acquires a long oscillatory tail, the frequency of which depends on time.

Keywords: THz surface plasmon waves; dispersive propagation; dielectric coating; chirped signal

1. Introduction

Efficient transmission of terahertz radiation is one of the challenges for the new generation of terahertz systems. To transmit terahertz pulses, waveguides with low losses and low dispersion are needed. Conventional dielectric fibers for visible light and metal waveguides for microwave radiation are unsuitable for use in the THz range. It is well known that SPPs in the THz frequency range are characterized by very low losses and have low dispersion [1–4]. Therefore, metal wire waveguides are very important for use in imaging, sensing and spectroscopy. Unlike SPPs in the visible and infrared frequency ranges [5–8], the propagation characteristics of SPPs in the terahertz frequency range are different [2]. It was shown in [2] that the behavior of SPPs on cylindrical metal surfaces in the terahertz frequency range is dispersive and differs from that of surface plasmon waves on a flat surface. It was found in [3] that a thin dielectric film on top of the metal leads to the strong confinement of the SPP's field to the surface. In [4], the effect of a dielectric coating on THz surface plasmon pulse propagation along a copper wire was studied. Recent studies show that THz surface plasmon waves can propagate not only at the boundary between a metal and a dielectric layer, but also along line-guided metallic structures, such as grooves, stripes, gratings, graphene metasurfaces and gaps [9–19]. Detailed reviews on terahertz technology and SPWs in the THz regime are presented in [20–22]. Various THz optical fiber types including solid core fibers, tube fibers, porous-core fibers, anti-resonant fibers and metamaterial-based fibers are examined in [23,24]. In [25], the propagation of surface plasmon polariton waves of a given frequency ω in the THz frequency range in metal wires with a dielectric coating were studied. It has been shown that the phase velocity decreases and the propagation length of SPWs increases if the wire is coated. However, the study of the propagation of pulses is of practical interest. When pulses propagate, noticeable changes occur. The fact is that the dependence of the speed and attenuation length on the frequency leads to the dispersive propagation of the pulse.

The velocity dispersion is a significant obstacle that limits the application of waveguides in terahertz communication systems and spectroscopy. The fact is that the various frequency components of a wide spectrum of THz radiation propagate at different group

velocities, which leads to the distortion of the pulse shape. The investigation of the dispersion properties of SPPs in the terahertz frequency range is of practical interest for various applications, such as waveguides, sensors, and communications. Coated metal wires can be used as sensitive sensors of the characteristics of dielectric materials at terahertz frequencies.

In this paper, we investigate the dispersive propagation of surface plasmon–polariton pulses along a coated metal wire in the terahertz frequency range. The effect of a dielectric coating made of a non-dispersive material on the dispersion of pulses is investigated. Analytical expressions for the electric field are obtained, which make it possible to carry out time-saving calculations of the characteristics of the pulse propagating along a coated wire. The origin of the experimentally observed long-chirped tail in a signal propagating along a coated metal wire is clarified.

2. Problem Formulation

Dielectric fibers are widely used to transmit electromagnetic beams in optical regimes through dielectric fibers [26,27]. Even though dielectric fibers for visible light cannot be used to transmit terahertz electromagnetic waves, the methods used to solve Maxwell's equations in the optical range can also be applied to consider terahertz radiation.

Below, we consider a cylindrical metal wire (Figure 1) of radius r_0, covered with a dielectric layer of radius $R_f \gg r_0$.
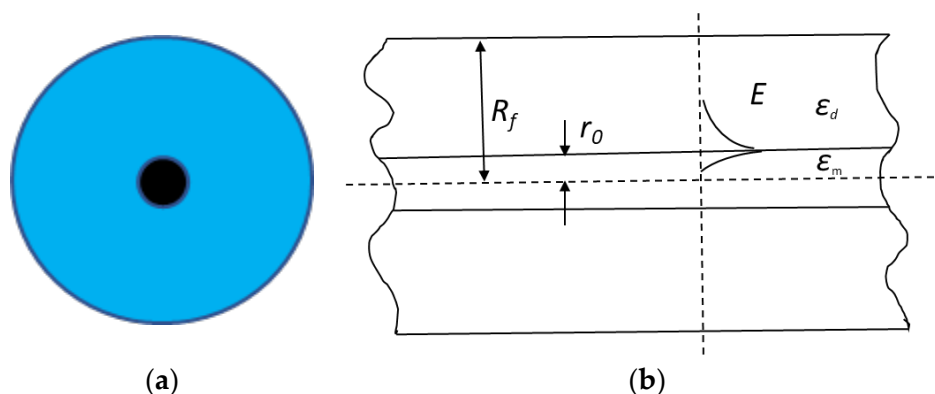

Figure 1. Cross section (**a**) and a side view (**b**) of a coated metal wire.

The propagation of surface electromagnetic waves along a conducting wire has long been well studied [28].

The guided modes of a coated cylindrical wire can be determined from the solution of the Helmholtz equations [29]:

$$\left[\nabla_\perp^2 + \left(k_0^2 \varepsilon_m - \beta^2\right)\right] E_z = 0, \; 0 < r < r_0$$

$$\left[\nabla_\perp^2 + \left(k_0^2 \varepsilon_d - \beta^2\right)\right] E_z = 0, \; r > r_0 \tag{1}$$

where $\nabla_\perp^2 = \frac{1}{r}\frac{\partial}{\partial r}\left(r\frac{\partial}{\partial r}\right) + \frac{1}{r^2}\frac{\partial^2}{\partial \varphi^2}$, $k_0 = \frac{\omega}{c}$ is the wavenumber in free space, β is the longitudinal component of the wavenumber, E_z is the longitudinal field component, r_0 is the metal wire radius, $\varepsilon_m = \varepsilon' + i\frac{\sigma}{\omega\varepsilon_0}$ is the complex dielectric constant, $\sigma = \frac{1}{R_l \pi r_0^2}$ is the conductivity of the wire, R_l is the resistance per unit length, ε_d is the dielectric constant of dielectric cover and ε_0 is the dielectric constant of free space.

Solutions of Equation (1) are expressed as:

$$E_z(z) = \begin{Bmatrix} A_1 I_0(\eta r), r \leq r_0 \\ A_2 K_0(\eta_0 r), r \geq r_0 \end{Bmatrix} e^{i\beta z} \tag{2}$$

where I_0 and K_0 are the modified Bessel functions of the first and second kind, A_1 and A_2 are the amplitude coefficients and $\eta^2 = \left(\frac{\omega^2}{c^2}\right)\varepsilon_p - \beta^2$, $\eta_0^2 = \left(\frac{\omega^2}{c^2}\right)\varepsilon_d - \beta^2$.

The propagation characteristics of the surface electromagnetic waves are determined via the dispersion equation:

$$\frac{\varepsilon_p}{\eta a}\frac{I_0'(\eta a)}{I_0(\eta a)} = \frac{1}{\eta_0 a}\frac{K_0'(\eta_0 a)}{K_0(\eta_0 a)} \tag{3}$$

where I_0 and K_0 are the modified Bessel functions of the first and second kind, and accordingly, I_0' and K_0' are the derivatives of the Bessel functions.

The spatial distribution of a surface wave of a given frequency is preserved during propagation. However, when pulses propagate, noticeable changes occur due to the dependence of speed on frequency. This leads to the dispersive propagation of the pulse.

Consider an input pulse in the form:

$$E(z = 0, t) = A_0 E(r) exp\left(-\frac{t^2}{\tau_0^2} + i\omega_0 t\right) = A_0 E(r) e^{i\omega_0 t} \int F(\widetilde{\Omega}) e^{i\widetilde{\Omega}t} d\widetilde{\Omega} \tag{4}$$

where $F(\widetilde{\Omega})$ is the spectrum of the incident pulse and $\widetilde{\Omega} = \omega - \omega_0$ is the detuning from the carrier frequency of the pulse ω_0.

The frequency spectrum of the pulse is determined by

$$F(\omega - \omega_0) = \frac{1}{\sqrt{2\pi}}\int_{-\infty}^{\infty} f(t)e^{-i\omega t}dt = \frac{\tau}{\sqrt{2\pi}}exp\left[-(\omega - \omega_0)^2\tau^2/2\right] \tag{5}$$

The spatial distribution of the field at $r \geq r_0$ can be expressed as an expansion in terms of plane waves

$$E(r, z, \omega - \omega_0) = A_2 \int_0^{\eta 0max} \eta_0 K_0(\eta_0 r) F(\omega - \omega_0) e^{i\beta(\omega)z} d\eta_0 \tag{6}$$

The inverse Fourier transform of (6) gives an expression for the electric field in the time domain:

$$E(r, z, t) = \frac{1}{2\pi}\int_{-\infty}^{\infty} E(r, z, \omega - \omega_0) exp[-i(\omega - \omega_0)t]d\omega \tag{7}$$

Expand $\beta(\omega)$ in a Taylor series in the neighborhood of ω_0:

$$\beta(\omega) = \sum_{m=0} \frac{(\omega - \omega_0)^m}{m!}\gamma_m = \gamma_0 + (\omega - \omega_0)\gamma_1 + \frac{(\omega - \omega_0)^2}{2!}\gamma_2 + \frac{(\omega - \omega_0)^3}{3!}\gamma_3 \cdots \tag{8}$$

where $\gamma_m = \frac{d^m}{d\omega^m}\beta(\omega)_{|\omega = \omega_0} = \omega_0$, $\gamma_1 = \frac{d\beta}{d\omega}_{|\omega = \omega_0}$.

Substituting (6) into (7), for the electric field, we obtain:

$$E(r, z, t) = \frac{\tau}{\sqrt{2\pi}}\int_0^{\eta 0max} \eta_0 K_0(\eta_0 r) e^{i\gamma_0 z} f(t, z, \tau) d\eta_0 \tag{9}$$

where $f(t, z, \tau) = \sqrt{\frac{2\pi}{\tau^2 - iz\gamma_2}}exp\left[-\frac{(t - z\gamma_1)^2}{2(\tau^2 - iz\gamma_2)}\right]$.

Here, the second-order dispersion term γ_2 is considered.

Considering the higher-order dispersion term γ_3 (third-order correction from (8)), we have

$$f(t,z,\tau) = \frac{2\pi}{\sqrt[3]{\gamma_3 z/2}} exp\left[\frac{1}{\gamma_3 z}(\gamma_1 z - t)\left(\tau^2 - i\gamma_2 z\right) + \frac{1}{3(\gamma_3 z)^2}\left(\tau^2 - i\gamma_2 z\right)^3\right] Ai(x) \quad (10)$$

where $Ai(x) = \frac{1}{2\pi}\int_{-\infty}^{\infty} exp\left(\frac{it^3}{3} + ixt\right)dt$ is the Airy function,

$$x = \frac{i}{\sqrt[3]{\gamma_3 z/2}}(\gamma_1 z - t) + \frac{1}{4(\gamma_3 z/2)^{4/3}}\left(\tau^2 - i\gamma_2 z\right)^2$$

The dispersion determined by the value of γ_2 leads to an increase in the pulse duration. A higher-order dispersion determined by the contribution of the γ_3 leads to a distortion of the pulse shape. The values of γ_1, γ_2 and γ_3 are defined by the propagation constant $\beta(\omega)$, which, in turn, is determined from the solution of the dispersion equation in Equation (3). The pulse acquires an asymmetric shape and has an oscillatory structure on the tail. Indeed, expression (10) for the electric field includes the Airy function, which is characterized by oscillatory behavior.

Note that the higher-order dispersion effects become significant if the dispersion length $L_3 = \tau^3/|\gamma_3|$ is less than the dispersion length $L_2 = \tau^2/|\gamma_2|$, i.e., when $\tau|\gamma_2/\gamma_3| < 1$. Usually, the contribution of the dispersion term γ_3 is small in comparison with the dispersion term γ_2. However, for the picosecond pulses in the terahertz range, the effect of the term γ_3 can be significant.

3. Pulse Velocity and Dispersion

The phase and group velocities of the SPWs can be determined from the dispersion equation in Equation (3). The phase velocity $V_{ph} = \frac{\omega}{\beta'}$ of the wave is defined by the real part of the propagation constant β', and the group velocity is determined by $V_g = \frac{d\omega}{d\beta'}$. The imaginary part β'' defines the attenuation length $z_0 = \frac{1}{\beta''}$ of the surface wave propagating along the wire.

Figure 2 shows the velocity and attenuation length depending on the frequency. The velocity increases and the propagation length decreases with increasing frequency. This indicates that propagation losses increase with increasing frequency, as in periodic structures [15–19].

It is seen that the speed increases and the propagation length decreases with increasing frequency. The velocity of propagation along a bare wire approaches the speed of light in free space. In a coated wire, the maximum speed is limited by the value $v_p = c/\sqrt{\varepsilon_d}$. The simulation shows that the propagation distance in a coated metal wire is longer than along a bare wire. An increase in the propagation length in the presence of a dielectric coating was also experimentally shown in [30].

The conductivity of metal wires can be determined from a Drude formula. For copper [31], the dielectric constant $\varepsilon_m = -6.3 \times 10^5 + i2.77 \times 10^6$ for the frequency of 0.5 THz. The conductivity of copper wire is $\sigma = 1.23 \times 10^7 \Omega^{-1} m^{-1}$. Slightly higher conductivity levels correspond to silver and gold wires.

3.1. Propagation along a Bare Wire

In Figure 3, the pulse intensities $I(z,t,\tau) = |E(z,t,\tau)|^2$ for different lengths of bare wires are presented in an offset time scale $t + T_0$, where $T_0 = z/v_p - 8\tau$, z is the distance at which the pulse is recorded. The values of γ_1, γ_2 and γ_3 are determined by the propagation constant $\beta(\omega)$, the real and imaginary parts of which determine the phase velocity and attenuation length of SPPs, respectively (Figure 2).
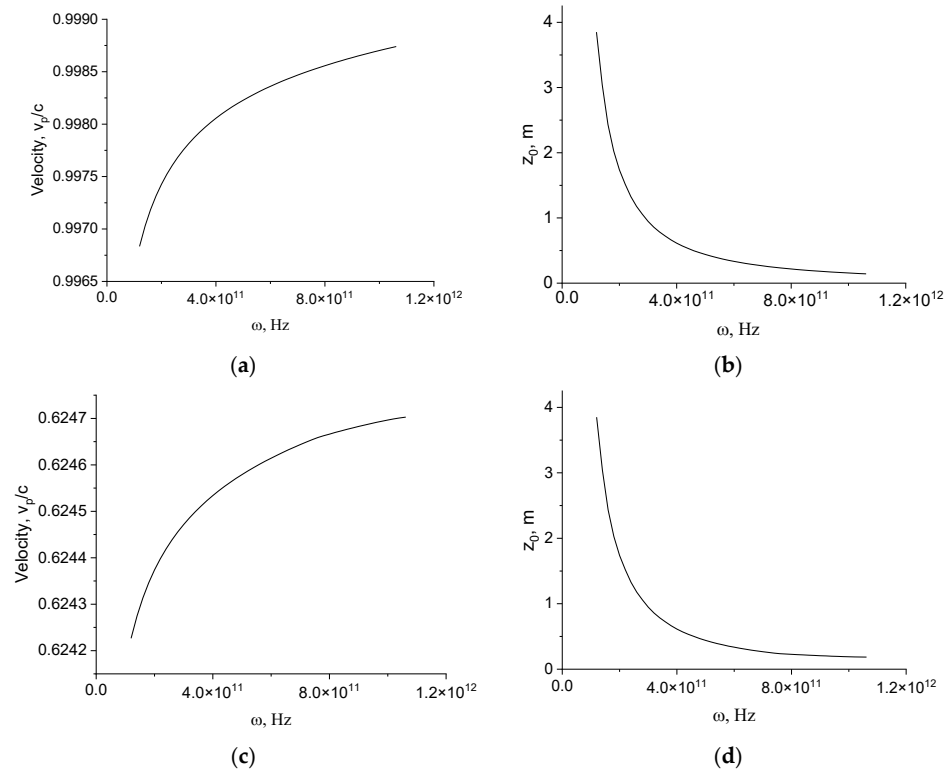
Figure 2. Phase velocity (**a**,**c**) and attenuation length (**b**,**d**) as function of frequency. $r_0 = 10$ μm. $\sigma = 1.23 \times 10^7 \Omega^{-1} \mathrm{m}^{-1}$. $\varepsilon_d = 1.0$ (**a**,**b**); $\varepsilon_d = 2.56$ (**c**,**d**).
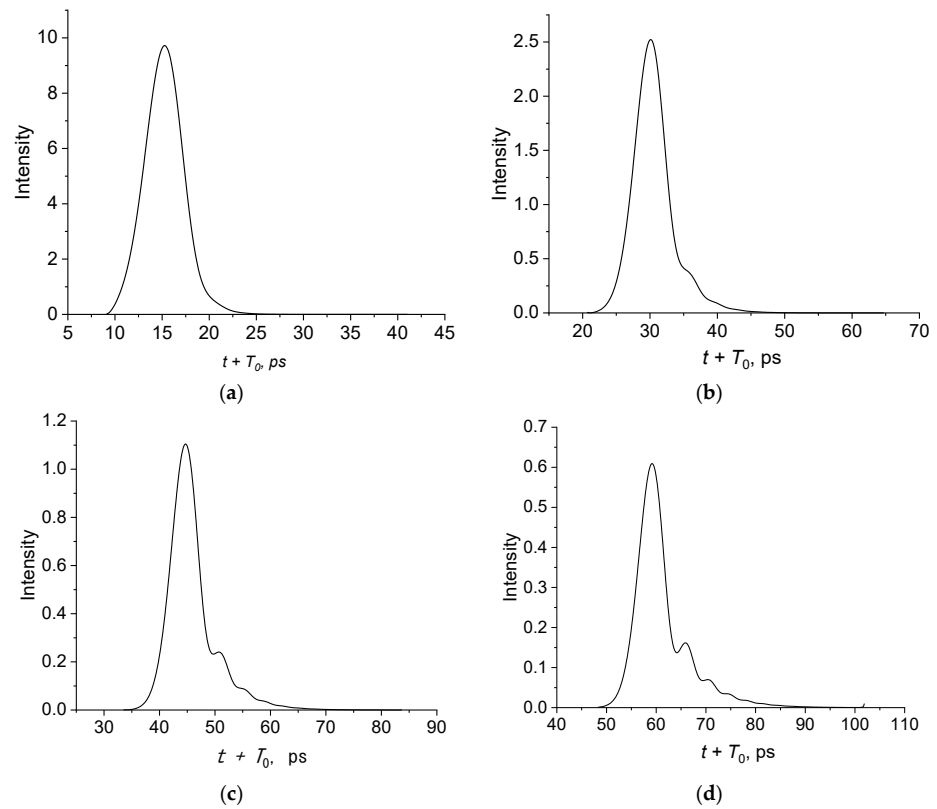

Figure 3. Intensity profiles of pulses at different lengths of bare wires. $z = 0.5$ cm (**a**), 1.0 cm (**b**), 1.5 cm (**c**) and 2.0 cm (**d**). $r_0 = 100$ μm. $\omega_0 = 0.8$ THz, $\tau = 2.3$ps, $\varepsilon_d = 1.0$, $T_0 = z/v_p - 8\tau$.

It can be seen that the shape of the pulse changes with distance, acquiring an asymmetric distribution. With increasing distance, the pulse amplitude decreases, while acquiring a long tail.

3.2. Effect of a Dielectric Coating

The dielectric coating affects the speed and length of the attenuation of surface waves. Glass and polymer materials were considered for use in the terahertz range [23,24,32]. Below, we use a constant refractive index $n = 1.6 + 0.03i$ in the calculations. This refractive index corresponds to the value for polyurethane given in [33] for the terahertz frequency range.

In Figure 4, the pulse intensity profiles at various distances for a given pulse duration and carrier frequency are presented.
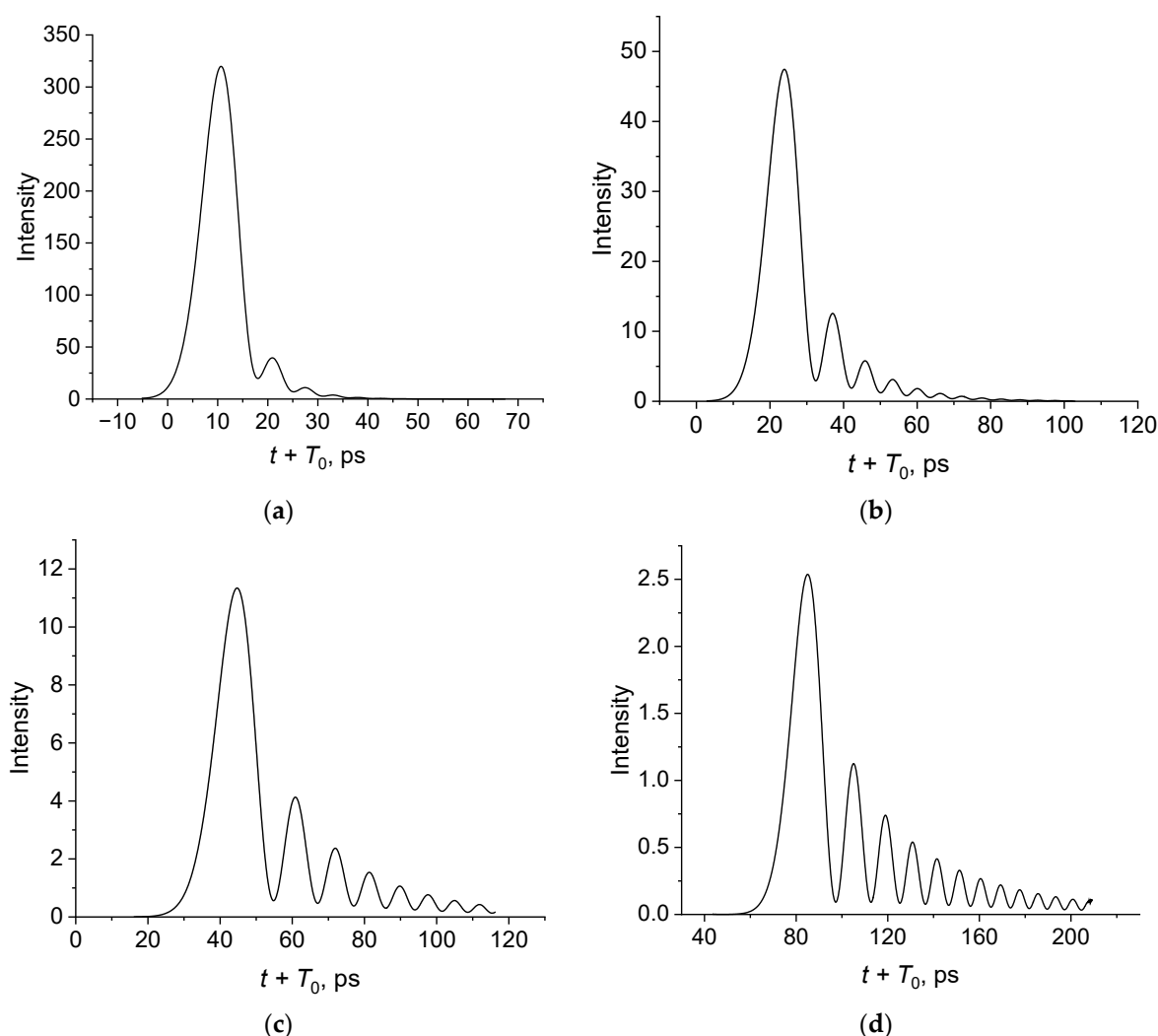

(**a**)

(**b**)

(**c**)

(**d**)

Figure 4. Intensity profiles of pulses at different distances. z = 0.1 cm (**a**), 0.25 cm (**b**), 0.5 cm (**c**) and 1.0 cm (**d**); r_0. = 100 μm, $\omega_0 = 0.9$ THz, $\tau = 3.5$ ps, $\varepsilon_d = 2.56$, $T_0 = z/v_p - 3\tau$.

Unlike a bare wire (Figure 3), propagation along a coated wire is highly dispersive (Figure 4). The coating leads to the appearance of a long-chirped signal with a propagation of only a few millimeters. The pulse amplitude decreases significantly with increasing distance. The appearance of the oscillatory tail in the pulse is caused by the third-order term γ_3 in (8). When only the second-order term γ_2 is considered, the pulse shape remains Gaussian. Note that such oscillatory behavior was also observed experimentally during the propagation of a terahertz pulse along a coated copper wire in [4].

3.3. Effect of a Pulse Duration

Consider the effect of the pulse duration on the shape of the pulse propagating along the coated wire. Figure 5 shows the pulse shapes for different durations of the incident pulse at a propagation distance of z = 0.5 cm.
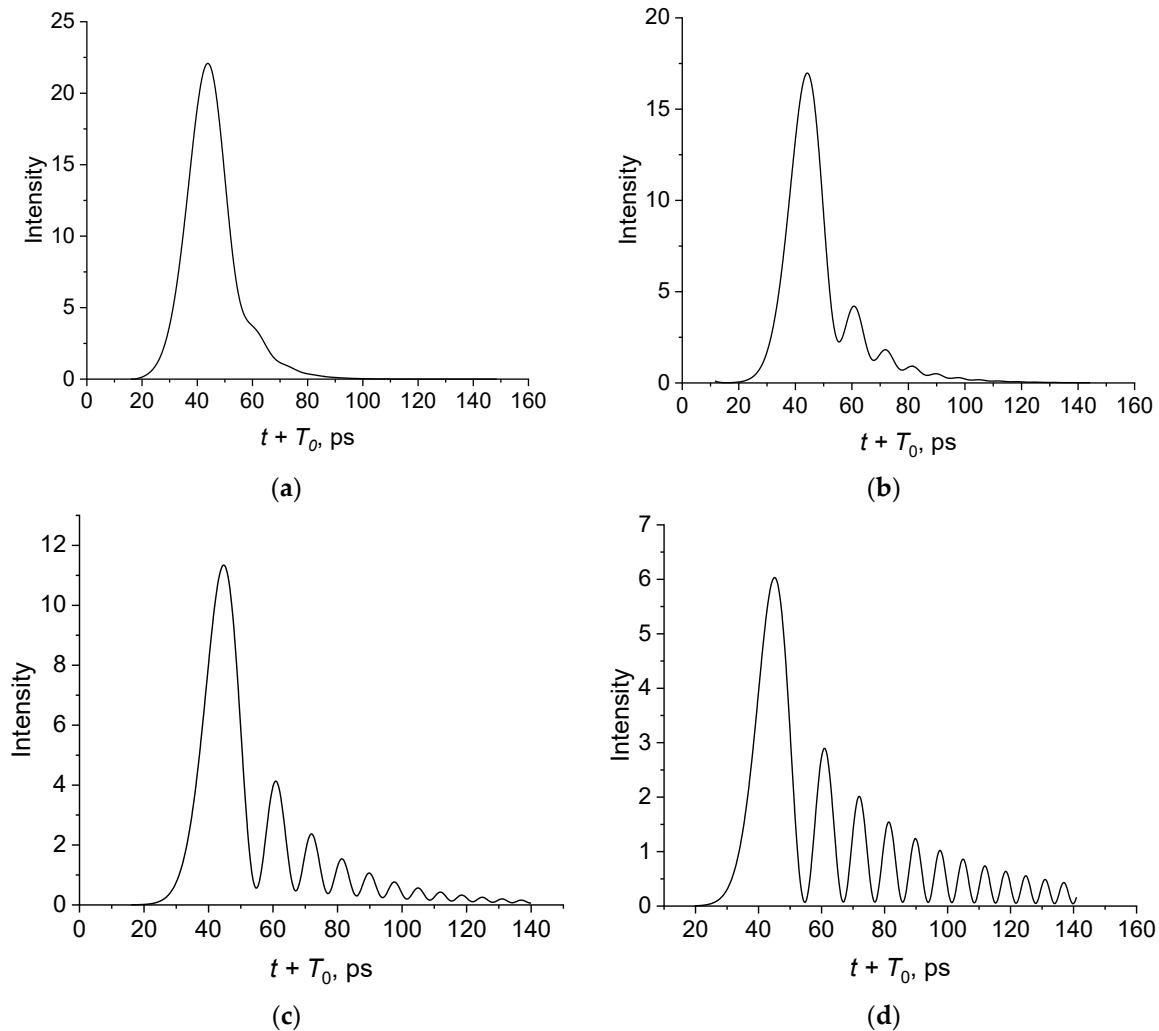
(a)

(b)

(c)

(d)

Figure 5. Intensity profiles of pulses for different incident pulse durations at z = 0.5 cm. τ = 7.0 ps (**a**), τ = 5.0 ps (**b**), τ = 3.5 ps (**c**), τ = 2.3 ps (**d**). r_0 = 100 μm, ω_0 = 0.9 THz, ε_d = 2.56, $T_0 = z/v_p - 3\tau$.

It follows from the simulation that the chirped output signal is observed when the pulse duration decreases, i.e., when the pulse width $\tau \cdot c$ becomes less than the carrier wavelength $\lambda_0 = 2\pi c/\omega_0$. For the pulse duration τ = 3 ps, the pulse width is equal to l_p = 0.9 mm. The carrier frequency of 0.9 THz corresponds to the carrier wavelength λ_0 = 2.1 mm. The oscillation depth increases as the pulse duration decreases. This indicates that the contribution of the dispersion term of the third order becomes significant with a decrease in the pulse duration. For a wide pulse, the third-order dispersion effect is negligible, and the oscillating tail disappears (Figure 5a).

4. Discussion

Thus, the effect of a dielectric coating on the dispersion of pulses propagating along a metal wire is investigated. The nondispersive coating material leads to highly dispersive propagation along the wire, which is expressed in the appearance of a chirped output signal. The results obtained are consistent with the experimental data presented in [4],

where the chirped signal was observed on the propagation of terahertz pulses over copper wire with a polyurethane coating.

The physical origin of the long-chirped tail is associated with a third-order dispersion term in the propagation constant (8). The oscillations at the tail of the pulse weaken with an increase in the incident pulse duration. This is due to the fact that as the pulse duration increases, the contribution of the dispersion term γ_2 becomes greater than that of the dispersion term γ_3. There is no oscillatory tail if the third-order dispersion term is neglected during modeling.

Note that the change in the shape of the pulse during propagation can be obtained from the time-consuming numerical solution of Maxwell's equations. Here, we used an analytical approach that allowed us to consider the effects of high-order dispersion leading to the appearance of a chirped signal observed in the experiments [4].

Losses in the dielectric coating are the main limitations to the transmission of a THz signal over long distances. Currently, porous-core photonic crystal fibers with a very low level of material loss were proposed for pulse propagation [34–37]. In [36], a photonic crystal structure with an average power loss of 0.02 cm^{-1} was designed and manufactured for THz radiation transmission.

Future research can be related to the consideration of pulse propagation taking into account higher-order dispersion terms and vortex modes of SPPs. Considering higher-order dispersion terms will allow us to analyze the propagation of very short pulses. The consideration of structured vortex beams with orbital angular momentum [33,38–40] and the effects of the Goos–Hanchen shift [41–43] is of great interest. Tunable resonance Goos–Hanchen and Imbert–Fedorov shifts for THz beams reflected from graphene plasmonic metasurfaces were investigated in [41]. It is expected that considering new additional parameters will allow us to detect new effects that are important for a new generation of terahertz systems.

5. Conclusions

In conclusion, the propagation characteristics of SPP pulses in the THz frequency range in cylindrical metal wires with a dielectric coating were studied through the analytical solution of Maxwell's equations. The expression was obtained for a pulsed electric field, taking into account high-order dispersion terms. This allowed for time-saving calculations of pulse propagation along a coated wire to be made.

It is shown that significant distortions of the terahertz pulse occur because of the dispersive propagation of SPPs along the coated wire. The coating results in a long-chirped signal for short-incident pulses. The depth of the oscillations strongly depends on the pulse duration, and the intensity can drop to zero between adjacent periods.

It follows from the study that coated metal wires can be used as sensitive sensors of the characteristics of dielectric materials at terahertz frequencies.

The results obtained can be applied in the field of THz spectroscopy and imaging, communications and plasmon fibers and in the development of various sensors.

Data Availability Statement: Not applicable.

Conflicts of Interest: The author declares no conflict of interest.

References

1. Wang, K.; Mittleman, D.M. Metal wires for terahertz wave guiding. *Nature* **2004**, *432*, 376–379. [CrossRef]
2. Wang, K.; Mittleman, D.M. Dispersion of surface plasmon polaritons on metal wires in the terahertz frequency range. *Phys. Rev. Lett.* **2006**, *96*, 157401. [CrossRef] [PubMed]
3. Saxler, J.; Rivas, J.G.; Janke, C.; Pellemans, H.P.M.; Bolivar, P.H.; Kurz, H. Time-domain measurements of surface plasmon polaritons in the terahertz frequency range. *Phys. Rev. B* **2004**, *69*, 155427. [CrossRef]

4. Van der Valk, N.C.J.; Planken, P.C.M. Effect of a dielectric coating on terahertz surface plasmon polaritons on metal wires. *Appl. Phys. Lett.* **2005**, *87*, 071106. [CrossRef]

5. Bessel, P.; Niebur, A.; Kranz, D.; Lauth, J.; Dorfs, D. Probing Bidirectional Plasmon-Plasmon Coupling-Induced Hot Charge Carriers in Dual Plasmonic Au/CuS Nanocrystals. *Small* **2023**, *19*, 2206379. [CrossRef]

6. Yi, R.; Wu, W.; Zhang, X. Femtosecond Autocorrelation of Localized Surface Plasmons. *Nanomaterials* **2023**, *13*, 1513. [CrossRef]

7. Beiranvand, B.; Sobolev, A.S. A proposal for a multi-functional tunable dual-band plasmonic absorber consisting of a periodic array of elliptical grooves. *J. Opt.* **2020**, *22*, 105005. [CrossRef]

8. Ntemogiannis, D.; Floropoulos, P.; Karoutsos, V.; Grammatikopoulos, S.; Poulopoulos, P.; Alexandropoulos, D. Plasmonic Nanostructuring by Means of Industrial-Friendly Laser Techniques. *Photonics* **2023**, *10*, 384. [CrossRef]

9. Mitrofanov, O.; Harrington, J.A. Dielectric-lined cylindrical metallic THz waveguides: Mode structure and dispersion. *Opt. Express* **2010**, *18*, 1898–1903. [CrossRef]

10. Chen, Y.; Song, Z.; Li, Y.; Hu, M.; Xing, Q.; Zhang, Z.; Chai, L.; Wang, C.Y. Effective surface plasmon polaritons on the metal wire with arrays of subwavelength grooves. *Opt. Express* **2006**, *14*, 13021–13029. [CrossRef]

11. Williams, C.R.; Andrews, S.R.; Maier, S.; Fernandez-Dominguez, A.I.; Martín-Moreno, L.; Garcia-Vidal, F. Highly confined guiding of terahertz surface plasmon polaritons on structured metal surfaces. *Nat. Photonics* **2008**, *2*, 175–179. [CrossRef]

12. Rivas, J.G.; Kuttge, M.; Bolivar, P.H.; Kurz, H.; Sánchez-Gil, J.A. Propagation of surface plasmon polaritons on semiconductor gratings. *Phys. Rev. Lett.* **2004**, *93*, 256804. [CrossRef] [PubMed]

13. Gan, C.H.; Chu, H.S.; Li, E.P. Synthesis of highly confined surface plasmon modes with doped graphene sheets in the midinfrared and terahertz frequencies. *Phys. Rev. B* **2012**, *85*, 125431. [CrossRef]

14. Bulgakova, V.V.; Gerasimov, V.V.; Goldenberg, B.G.; Lemzyakov, A.G.; Malkin, A.M. Study of terahertz spoof surface plasmons on subwavelength gratings with dielectric substance in grooves. *Phys. Procedia* **2017**, *201*, 14–23. [CrossRef]

15. Liu, Y.Q.; Kong, L.B.; Du, C.H.; Liu, P.K. Spoof surface plasmon modes on doubly corrugated metal surfaces at terahertz frequencies. *J. Phys. D Appl. Phys.* **2016**, *49*, 235501. [CrossRef]

16. Liu, Y.-Q.; Sun, J.; Li, L.; Yin, H. Asymmetric propagation of spoof surface plasmons along doubly corrugated metal surfaces. *AIP Adv.* **2020**, *10*, 045005. [CrossRef]

17. Liu, Y.Q.; Li, L.; Yin, H. Surface plasmon dispersion and modes on the graphene metasurface with periodical ribbon arrays. *Mater. Res. Express* **2020**, *7*, 075801. [CrossRef]

18. Liu, Y.-Q.; Li, L.; Yin, H. Long-range spoof surface plasmons (LRSSP) on the asymmetric double metal gratings. *IEEE Photon. J.* **2021**, *13*, 4800209. [CrossRef]

19. Liu, Y.-Q.; Ren, Z.; Yin, H.; Sun, J.; Li, L. Dispersion Theory of Surface Plasmon Polaritons on Bilayer Graphene Metasurfaces. *Nanomaterials* **2022**, *12*, 1804. [CrossRef]

20. Dhillon, S.S.; Vitiello, M.S.; Linfield, E.H.; Davies, A.; Hoffmann, M.; Booske, J.; Paoloni, C.; Gensch, M.; Weightman, P.; Williams, G.P.; et al. The 2017 terahertz science and technology roadmap. *J. Phys. D Appl. Phys.* **2017**, *50*, 043001. [CrossRef]

21. Chen, S.H.; Chen, K.W.; Chu, K.R. A comparative study of single-wire and hollow metallic waveguides for terahertz waves. *AIP Adv.* **2018**, *8*, 115028. [CrossRef]

22. Zhang, X.; Xu, Q.; Xia, L.; Li, Y.; Gu, J.; Tian, Z.; Ouyang, C.; Han, J.; Zhang, W. Terahertz surface plasmonic waves: A review. *Adv. Photonics* **2020**, *2*, 014001. [CrossRef]

23. Atakaramians, A.; Afshar, S.V.; Monro, T.M.; Abbott, D. Terahertz dielectric waveguides. *Adv. Opt. Photon.* **2013**, *5*, 169–215. [CrossRef]

24. Islam, M.S.; Cordeiro, C.M.B.; Franco, M.A.R.; Sultana, J.; Cruz, A.L.S.; Abbott, D. Terahertz optical fibers [Invited]. *Opt. Express* **2020**, *28*, 16089–16117. [CrossRef] [PubMed]

25. Petrov, N.I. Propagation of Terahertz Surface Plasmon Polaritons in a Dielectric Fiber with a Metal Wire Core. *Fibers* **2022**, *10*, 89. [CrossRef]

26. Marcuse, D. *Light Transmission Optics*; Van Nostrand Reinhold: New York, NY, USA, 1982.

27. Snyder, A.W.; Love, J. *Optical Waveguide Theory*; Chapman and Hall: New York, NY, USA, 1983.

28. Sommerfeld, A. Ueber die Fortpflanzung elektrodynamischer Wellen längs eines Drahtes. *Ann. Phys.* **1899**, *303*, 233–290. [CrossRef]

29. Petrov, N.I. Synchrotron mechanism of X-ray and gamma-ray emissions in lightning and spark discharges. *Sci. Rep.* **2021**, *11*, 19824. [CrossRef]

30. Gerasimov, V.V.; Knyazev, B.A.; Lemzyakov, A.G.; Nikitin, A.K.; Zhizhin, G.N. Growth of terahertz surface plasmon propagation length due to thin-layer dielectric coating. *J. Opt. Soc. Am. B* **2016**, *33*, 2196–2203. [CrossRef]

31. Ordal, M.A.; Bell, R.J.; Alexander, R.W.; Long, L.L.; Querry, M.R. Optical properties of fourteen metals in the infrared and far infrared: Al, Co, Cu, Au, Fe, Pb, Mo, Ni, Pd, Pt, Ag, Ti, V, and W. *Appl. Opt.* **1985**, *24*, 4493–4499. [CrossRef] [PubMed]

32. Jin, Y.S.; Kim, G.J.; Jeon, S.G. Terahertz Dielectric Properties of Polymers. *J. Korean Phys. Soc.* **2006**, *49*, 513–517.

33. Stefani, A.; Fleming, S.C.; Kuhlmey, B.T. Terahertz orbital angular momentum modes with flexible twisted hollow core antiresonant fiber. *APL Photonics* **2018**, *3*, 051708. [CrossRef]

34. Hassani, A.; Dupuis, A.; Skorobogatiy, M. Porous polymer fibers for low-loss Terahertz guiding. *Opt. Express* **2008**, *16*, 6340–6351. [CrossRef] [PubMed]

35. Paul, B.K.; Bhuiyan, T.; Abdulrazak, L.F.; Sarker, K.; Hassan, M.M.; Shariful, S.; Ahmed, K. Extremely low loss optical waveguide for terahertz pulse guidance. *Results Phys.* **2019**, *15*, 102666. [CrossRef]
36. Yang, J.; Zhao, J.; Gong, C.; Tian, H.; Sun, L.; Chen, P.; Lin, L.; Liu, W. 3D printed low-loss THz waveguide based on Kagome photonic crystal structure. *Opt. Express* **2016**, *24*, 22454–22460. [CrossRef]
37. Stefani, A.; Skelton, J.H.; Tuniz, A. Bend losses in flexible polyurethane antiresonant terahertz waveguides. *Opt. Exp.* **2021**, *29*, 28692–28703. [CrossRef]
38. Petrov, N.I. Splitting of levels in a cylindrical dielectric waveguide. *Opt. Lett.* **2013**, *38*, 2020–2022. [CrossRef]
39. Petrov, N.I. Vector Laguerre–Gauss beams with polarization-orbital angular momentum entanglement in a graded-index medium. *J. Opt. Soc. Am. A* **2016**, *33*, 1363–1369. [CrossRef]
40. Petrov, N.I. Nonparaxial Propagation of Bessel Correlated Vortex Beams in Free Space. *Micromachines* **2023**, *14*, 38. [CrossRef]
41. Farmani, A.; Miri, M.; Sheikhi, M.H. Tunable resonant Goos–Hänchen and Imbert–Fedorov shifts in total reflection of terahertz beams from graphene plasmonic metasurfaces. *J. Opt. Soc. Am. B* **2017**, *34*, 1097–1106. [CrossRef]
42. Petrov, N.I.; Sokolov, Y.M.; Stoiakin, V.V.; Danilov, V.A.; Popov, V.V.; Usievich, B.A. Observation of Giant Angular Goos-Hanchen Shifts Enhanced by Surface Plasmon Resonance in Subwavelength Grating. *Photonics* **2023**, *10*, 180. [CrossRef]
43. Kan, X.F.; Zou, Z.X.; Yin, C.; Xu, H.P.; Wang, X.P.; Han, Q.B.; Cao, Z.Q. Continuous Goos-Hänchen Shift of Vortex Beam via Symmetric Metal-Cladding Waveguide. *Materials* **2022**, *15*, 4267. [CrossRef] [PubMed]